

Sparse inference and active learning of stochastic differential equations from data

Yunfei Huang,^{1,*} Youssef Mabrouk,^{2,3,*} Gerhard Gompper,¹ and Benedikt Sabass^{1,2,†}

¹*Theoretical Physics of Living Matter, Institute of Biological Information Processing and Institute for Advanced Simulation, Forschungszentrum Juelich, 52425 Juelich, Germany*

²*Institute for Infectious Diseases and Zoonoses, Department of Veterinary Sciences, Ludwig-Maximilians-Universitaet Munich, 80539 Munich, Germany*

³*Helmholtz Institute Muenster (HI MS), IEK-12 Forschungszentrum Juelich GmbH, Corrensstraße 46, 48149 Muenster, Germany*

(Dated: March 22, 2022)

Automatic machine learning of empirical models from experimental data has recently become possible as a result of increased availability of computational power and dedicated algorithms. Despite the successes of non-parametric inference and neural-network-based inference for empirical modelling, a physical interpretation of the results often remains challenging. Here, we focus on direct inference of governing differential equations from data, which can be formulated as a linear inverse problem. A Bayesian framework with a Laplacian prior distribution is employed for finding sparse solutions efficiently. The superior accuracy and robustness of the method is demonstrated for various cases, including ordinary, partial, and stochastic differential equations. Furthermore, we develop an active learning procedure for the automated discovery of stochastic differential equations. In this procedure, learning of the unknown dynamical equations is coupled to the application of perturbations to the measured system in a feedback loop. We demonstrate with simulations that the active learning procedure improves the inference of empirical, Langevin-type descriptions of stochastic processes.

I. INTRODUCTION

Throughout the natural sciences, mathematical models are frequently formulated as differential equations. For example, with stochastic, ordinary, and partial differential equations (SDEs, ODEs, and PDEs). In physics, governing differential equations are often derived from first principles, for instance, from conservation of energy, momentum, and thermodynamic considerations. However, for complex systems studied, e.g., in biophysics, climate science, and neuroscience, first principles determining the system properties are typically not fully known. For example, because such systems are in a driven non-equilibrium state, highly nonlinear, and because dynamics may occur on multiple scales that are not well separated. In these cases, one can resort to phenomenological, effective descriptions that may result from some level of coarse graining and are based on experimental data. Recently, the increased availability of computational power has made it possible to construct such models in an automated fashion, which is known as data-driven discovery of governing equations.

Various approaches have been developed for inferring the differential equations that govern a non-linear dynamical system directly from measured data [1–6]. In a popular approach called “symbolic regression”, function libraries are employed to automatically extract the terms in a governing equation that best represents the measured data according to some optimization criterion [1, 2]. Recently, the use of sparse regression techniques for sym-

bolic regression has received considerable scientific attention [3, 4]. In symbolic regression, the physical quantity z , which is for illustration taken to be a scalar here, is assumed to obey an equation of the general form

$$\dot{z} = \mathcal{F}(z, \mathbf{x}, t, c), \quad (1)$$

where \dot{z} can be, e.g., a time derivative $\dot{z} = \frac{\partial z}{\partial t}$ for ODEs and PDEs. $\mathcal{F}(z, \mathbf{x}, t, c)$ is an unknown function whose arguments \mathbf{x} represent space coordinates while t represents time and c is a constant parameter. The aim of symbolic regression is to estimate the function $\mathcal{F}(\dots)$ from a data set \mathbf{z} , which could be a measured sequence of values of z at different time-space coordinates. The vector $\dot{\mathbf{z}}$ is either measured or estimated from \mathbf{z} , e.g., with a discrete difference scheme. For inference of $\mathcal{F}(\dots)$, a so-called “library” $\Theta(\mathbf{z})$ is constructed from a suitable set of functions of \mathbf{z} , e.g., various powers of \mathbf{z} , combinations of partial derivatives, or trigonometric functions. Assuming that the governing equation (1) can be expressed as a linear superposition of library terms, we write

$$\dot{\mathbf{z}} = \Theta(\mathbf{z})\boldsymbol{\xi}, \quad (2)$$

where $\boldsymbol{\xi}$ is a weight vector. The inference of the governing equation is thus reduced to a regression problem for the optimal $\boldsymbol{\xi}$, given $\dot{\mathbf{z}}$ and $\Theta(\mathbf{z})$. In general, solving the inverse problem in Eq. (2) is not straight-forward since the matrix Θ should represent many equation terms and can have a large condition number $\kappa(\Theta)$.

In Ref. [3], a method called sparse identification of nonlinear dynamics (SINDy) has been proposed. The method works iteratively, where at each iteration $\boldsymbol{\xi}$ is first obtained from a least-squares optimization of Eq. (2) and subsequently $\boldsymbol{\xi}$ is thresholded such that values smaller

* Contributed equally

† E-mail address: b.sabass@lmu.de

than a cutoff κ are set to zero. The iteration is continued until convergence conditions are satisfied. SINDy has been shown to be a powerful and versatile method that is applicable for inference of various types of ODEs [3]. However, the method requires the user to manually select the thresholds κ . For the identification of PDEs, an alternative algorithm called train sequential threshold ridge regression (TrainSTRidge) has been described in Ref. [4]. This method is a variant of a least-squares optimization procedure for ridge regression called Sequential Threshold Ridge regression (STRidge). In STRidge, the vector ξ is first calculated by using ridge regression with a fixed regularization parameter. Then, all elements in ξ that have a smaller absolute value than a threshold κ are set to zero. Both, the regularization parameter and the threshold κ need to be provided by the user in STRidge. TrainSTRidge [4] employs L0 regularization and a training step to automatically determine the threshold κ while the regularization parameter remains to be set by the expert user. Conversely, a method called threshold sparse Bayesian regression, which also was employed for identification of PDEs [7], requires no input of a regularization parameters but some thresholds remain to be provided by the user.

The first aim of this work is to provide a method to solve the inverse problem associated with data-driven discovery of governing physical equations, Eq. (2), by combining a Bayesian approach with a automatic thresholding procedure. We call this method *automatic threshold sparse Bayesian learning* (ATSBL). Our algorithm does not require any manual fine-tuning of parameters to correctly infer governing differential equations from measured data. The method can be employed to identify ODEs, PDEs, and SDEs.

The case of SDEs requires particular attention, since the above-mentioned methods of equation inference are mainly designed for deterministic processes and some moderate amount of additive noise. The question how to reconstruct the force fields for stochastic processes has been investigated in numerous studies for application in soft matter physics and biophysics [5, 8–12]. Recently, sophisticated methods have been proposed for dealing with discretization and the inference problem in the context of SDEs for second-order dynamics [13–16]. Here, we focus on the use of symbolic regression for the inference of analytical expressions of SDEs of the overdamped Langevin-type. One approach to symbolic regression in this context is based on dividing the phase space into small hypercubes, also called bins in the one dimensional case. Average values of the state variables and of their derivatives are estimated in each hypercube and the regression is defined with respect to these averages [5]. This kind of averaging generally depends on the chosen discretization and the averaging may lead to a substantial loss of information. Furthermore, application of this method to non-stationary processes requires a large ensemble of trajectories and considerable numerical effort to sample the time-dependent probability distribution in phase space.

The difficulties related to the averaging in phase space motivate the investigation of the question to what extent the above-mentioned inference tools can be used in the context of noisy data without the need to perform *ad hoc* averaging, and, eventually, how the robustness of the inference methods may be improved in this context. We show that imposing Laplacian or Gaussian prior distributions on the inferred models is generally sufficient to identify the correct SDEs directly from trajectories without phase-space binning and we provide a comparison of the accuracy of results obtained with the two types of prior distributions. A remarkable performance of the Laplacian prior is demonstrated with several examples, including Brownian motion in time-dependent potentials.

A major challenge for the inference of SDEs is that the phase space is often sampled very inhomogeneously in available data. This problem is encountered, e.g., for systems where the long-term dynamics is dominated by transitions between different, locally stable states, while the short-term dynamics are dominated by fluctuations around individual stable states. In such cases, the inferred equation may be meaningful only locally, i.e. within the region covered by the measurement trajectory, and it may be *a priori* impossible to infer the global dynamics from a given data set. To enable an automatic inference of a global model under these conditions, we consider the question of how to design an external perturbation to the system, also called “control force”, such that the state variables are forced to explore the full phase space in a shortened sampling time. Standard Umbrella sampling routines used for this purpose rely on quadratic control forces and involve non-trivial design steps for the control force [17–20]. See, e.g., Refs. [21, 22] for alternative approaches. We develop an alternative adaptive control technique that recursively infers the governing equation and adapts the external control solely based on inferred equations. The adaptation loop consists of inference of the governing equation and a subsequent update of the control force such that it is directly opposite to the inferred force. No parameters need to be tuned for designing the control with this adaptive scheme. Using the adaptive control scheme, we demonstrate a substantial improvement of the inference of SDEs for several different simulations of Brownian motion.

This work is organized as follows. In Sec. 2, the construction of function libraries and the casting of the inference problem into a system of linear equations is described. Then, the inference algorithm is summarized, and it is explained how Laplacian prior distributions can be used to impose the sparsity condition on the inferred models. In Sec. 3, the performance of the described method is illustrated by means of numerical examples and a comparison with previously described methods is presented. An adaptive sampling technique for improving the inference of SDEs is proposed and the usefulness of this approach is demonstrated. Section 4 contains a short concluding perspective.

II. DATA-DRIVEN IDENTIFICATION OF DIFFERENTIAL EQUATIONS

A. Ordinary and partial differential equations

Measurement data from a system of interest is presumed to be recorded as a time series of states, for example, a time-dependent position vector. In a data-driven approach to model a system, the data is used to automatically infer the *a priori* unknown dynamical equations that govern the observed process. In this work, inference is based on libraries of candidate functions for the governing equations.

For inference of ODEs, a M -dimensional data vector $[z_1, z_2, \dots, z_M]$, recorded at times t_1, \dots, t_N , is assumed to be provided. Thus, the data can be written in a matrix form

$$\mathbf{Z} = [\mathbf{z}_1, \mathbf{z}_2, \dots, \mathbf{z}_M] = \begin{array}{c} \text{time} \\ \left[\begin{array}{cccc} z_1(t_1) & z_2(t_1) & \cdots & z_M(t_1) \\ z_1(t_2) & z_2(t_2) & \cdots & z_M(t_2) \\ \vdots & \vdots & \ddots & \vdots \\ z_1(t_N) & z_2(t_N) & \cdots & z_M(t_N) \end{array} \right] \end{array} \xrightarrow{\text{state}}$$

Time derivatives of the measurement data are calculated using with the finite difference approximation to obtain

$$\dot{\mathbf{Z}} = [\dot{\mathbf{z}}_1, \dot{\mathbf{z}}_2, \dots, \dot{\mathbf{z}}_M] = \begin{array}{c} \text{time} \\ \left[\begin{array}{cccc} \dot{z}_1(t_1) & \dot{z}_2(t_1) & \cdots & \dot{z}_M(t_1) \\ \dot{z}_1(t_2) & \dot{z}_2(t_2) & \cdots & \dot{z}_M(t_2) \\ \vdots & \vdots & \ddots & \vdots \\ \dot{z}_1(t_N) & \dot{z}_2(t_N) & \cdots & \dot{z}_M(t_N) \end{array} \right] \end{array} \xrightarrow{\text{state}}$$

A governing ODE for the vector containing the trajectory of the ℓ -th state component, \mathbf{z}_ℓ , $\ell \in \{1 \dots M\}$ may be written as a linear combination of elementary functions of all $\{\mathbf{z}_\ell\}$, e.g., as

$$\dot{\mathbf{z}}_\ell = \mathcal{F}_\ell(\mathbf{z}_1, \dots, \mathbf{z}_M, \mathbf{z}_1^2, \mathbf{z}_1 \mathbf{z}_2, \dots, \cos(\mathbf{z}_1), \dots, c), \quad (3)$$

where c represents a constant. The left-hand side of Eq. (3), $\dot{\mathbf{z}}_\ell$, is assumed to be known. Since $\mathcal{F}_\ell(\cdot)$ represents a linear combination of functions that can be calculated from the data, $\mathcal{F}_\ell(\cdot)$ can be expressed with the help of library matrix $\Theta(\mathbf{z})$ multiplied with a sparse vector ξ_ℓ . Thus, we obtain

$$\dot{\mathbf{z}}_\ell = \Theta(\mathbf{z}) \xi_\ell, \quad (4)$$

where the terms of the library matrix $\Theta(\mathbf{z})$ are calculated from the measurement data by evaluating the functions of $\{\mathbf{z}_{\ell'}\}$. Since Eq. (4) refers to ODEs here, no derivative terms are contained in the library on the right-hand side of the equation. Given $\dot{\mathbf{z}}_\ell$ and $\Theta(\mathbf{z})$, the aim is to calculate a sparse vector ξ_ℓ with a minimal number of non-zero coefficients corresponding to a minimal number of terms necessary to describe the dynamics.

For inference of PDEs, the library matrix Θ has to contain partial-derivative terms. Thus, data is required that allows the numerical estimation of derivative expressions with respect to two or more variables, for example, with respect to time and space. Usually, measurements therefore consist of discrete space-time series recordings of system variables. For example, an array \mathbf{Z}^P , representing an M -dimensional state measured at R positions of one space coordinate x and at N time points, is written as

$$\mathbf{Z}^P = \begin{array}{c} \text{time} \\ \left[\begin{array}{cccc} z_1(x_R, t_1) & z_2(x_R, t_1) & \cdots & z_n(x_R, t_1) \\ z_1(x_2, t_1) & z_2(x_2, t_1) & \cdots & z_M(x_2, t_1) \\ z_1(x_1, t_1) & z_2(x_1, t_1) & \cdots & z_M(x_1, t_1) \\ z_1(x_1, t_2) & z_2(x_1, t_2) & \cdots & z_M(x_1, t_2) \\ \vdots & \vdots & \ddots & \vdots \\ z_1(x_1, t_N) & z_2(x_1, t_N) & \cdots & z_M(x_1, t_N) \end{array} \right] \end{array} \xrightarrow{\text{state}}$$

(x_R, t₁)
(x_R, t₂)
⋮
(x_R, t_N)

With a finite-difference approximation, vectors of time derivatives of every component $\dot{\mathbf{z}}_\ell$ and various orders of x derivatives are calculated, for example, $(\mathbf{Z}^P)_x$, $(\mathbf{Z}^P)_{xx}$, \dots . These derivative terms are added to the library Θ^P . Like for ODEs, inference of the dynamical equation governing the component \mathbf{z}_ℓ is then based on the linear equation

$$\dot{\mathbf{z}}_\ell = \Theta^P [\mathbf{Z}^P, (\mathbf{Z}^P)_x, (\mathbf{Z}^P)_{xx}, \dots] \xi_\ell, \quad (5)$$

with a sparse coefficient vector ξ_ℓ to be determined.

B. Stochastic differential equations

We focus on Langevin-type SDEs to describe the time evolution of continuous, real state variables $\mathbf{X}(t)$, representing, e.g., the position of a Brownian particle in space [23, 24]. Trajectories, denoted by $\mathbf{X}(t)$, are time-ordered sequences of values of space coordinates \mathbf{x} . The general form of the considered SDEs is

$$dX_\ell(t) = \underbrace{g_\ell(\mathbf{X}(t), t) dt}_{\text{deterministic part}} + \underbrace{h_{\ell, \ell'}(\mathbf{X}(t), t) dW_{\ell'}(t)}_{\text{noise}}, \quad (6)$$

where we employ the Einstein sum convention and $X_\ell(t)$ denotes the ℓ -th component of the system state at time t . The trajectories \mathbf{X} are calculated by making use of Ito's interpretation of stochastic integrals [23]. The $g_\ell(\mathbf{X}(t), t)$ represent the deterministic parts of the differential equations. For example, for a Brownian particle undergoing overdamped motion in the presence of conservative forces with a potential $U(\mathbf{x}, t)$, we have $g_\ell(\mathbf{X}, t) = -\nabla_{x_\ell} U(\mathbf{x}, t)|_{\mathbf{x} = \mathbf{X}(t)}$. The stochastic perturbations to the trajectory $\mathbf{X}(t)$ are assumed to result from a Wiener process with a noise source $\Gamma_\ell(t)$ and $dW_\ell = \Gamma_\ell(t) dt$. The coefficient matrix $h_{\ell, \ell'}$ scales the

magnitude of the stochastic perturbations. The noise is assumed to obey a Gaussian distribution with a vanishing mean and a δ -correlated variance as

$$\langle \Gamma_\ell(t) \rangle = 0, \quad (7a)$$

$$\langle \Gamma_\ell(t) \Gamma_{\ell'}(t') \rangle = \delta_{\ell, \ell'} \delta(t - t'), \quad (7b)$$

respectively. The Fokker-Planck equation that corresponds to Eq. (6) and describes the evolution of a probability density function $f(\mathbf{x}, t)$ is given by

$$\frac{\partial f(\mathbf{x}, t)}{\partial t} = \hat{L}(\mathbf{x}, t) f(\mathbf{x}, t), \quad (8)$$

where the Fokker-Planck operator $\hat{L}(\mathbf{x}, t)$ [25] has the form

$$\hat{L}(\mathbf{x}, t) = -\frac{\partial}{\partial x_\ell} D_\ell^{(1)}(\mathbf{x}, t) + \frac{\partial^2}{\partial x_\ell \partial x_{\ell'}} D_{\ell, \ell'}^{(2)}(\mathbf{x}, t). \quad (9)$$

The functions $D_\ell^{(1)}(\mathbf{x}, t)$ and $D_{\ell, \ell'}^{(2)}(\mathbf{x}, t)$ are called Kramers-Moyal (KM) coefficients or drift and diffusion coefficients. Under the assumption of perfect knowledge of the trajectories $\mathbf{X}(t)$, the KM coefficients can be calculated from the incremental changes $\Delta X_\ell(t) \equiv X_\ell(t + \tau) - X_\ell(t)$ in an infinitesimal time interval τ as

$$D_\ell^{(1)}(\mathbf{x}, t) = \lim_{\tau \rightarrow 0} \frac{1}{\tau} \langle [\Delta X_\ell(t)] \rangle_{\mathbf{X}(t)=\mathbf{x}}, \quad (10a)$$

$$D_{\ell, \ell'}^{(2)}(\mathbf{x}, t) = \lim_{\tau \rightarrow 0} \frac{1}{2\tau} \langle [\Delta X_\ell(t)] [\Delta X_{\ell'}(t)] \rangle_{\mathbf{X}(t)=\mathbf{x}}, \quad (10b)$$

The KM coefficients are related to the functions g_ℓ and $h_{\ell, \ell'}$ in the Langevin equation as

$$g_\ell(\mathbf{x}, t) = D_\ell^{(1)}(\mathbf{x}, t), \quad (11a)$$

$$h_{\ell, \ell'}(\mathbf{x}, t) = \sqrt{2D_{\ell, \ell'}^{(2)}(\mathbf{x}, t)}. \quad (11b)$$

We consider only diagonal diffusion matrices, but the KM coefficients can depend explicitly on space and time. To estimate the coefficients with the help of Eqs. (10a, 10b), M -dimensional trajectories $X_{\ell, i}$, $\ell \in \{1, \dots, M\}$ are recorded with small time step s and a time-point index $i \in \{1, \dots, N\}$. Therewith, two new sequences are constructed as

$$\mathbf{F}_\ell^{(1)} = \{F_{\ell, i}^{(1)}\}_{i=1, \dots, N} = \left\{ \frac{X_{\ell, i+1} - X_{\ell, i}}{s} \right\}_{i=1, \dots, N}, \quad (12a)$$

$$\mathbf{F}_\ell^{(2)} = \{F_{\ell, i}^{(2)}\}_{i=1, \dots, N} = \left\{ \frac{(X_{\ell, i+1} - X_{\ell, i})^2}{2s} \right\}_{i=1, \dots, N}, \quad (12b)$$

where s is a small time step [5]. In the following, we employ two different methods for estimating the drift and diffusion coefficients. Firstly, a method is described in the next subsection that is based on binning of the data in phase space. Secondly, an approach is described that can be used to estimate the coefficients without data binning.

1. Estimation of KM coefficients from binned data

A classical method for the characterization of drift and diffusion parameters is based on binning the trajectory data in space intervals [5, 25–27]. For this approach, we focus on problems with only one space dimension ($M = 1$). To estimate probability distributions, the data is grouped into Q bins and the values in each bin are averaged as

$$\{X_i\}_{i=1, \dots, N} \mapsto \{\bar{X}_k\}_{k=1, \dots, Q} = \bar{\mathbf{X}}, \quad (13a)$$

$$\{F_i^{(1)}\}_{i=1, \dots, N} \mapsto \{\bar{F}_k^{(1)}\}_{k=1, \dots, Q} = \bar{\mathbf{F}}^{(1)}, \quad (13b)$$

$$\{F_i^{(2)}\}_{i=1, \dots, N} \mapsto \{\bar{F}_k^{(2)}\}_{k=1, \dots, Q} = \bar{\mathbf{F}}^{(2)}, \quad (13c)$$

where \bar{X}_k and $\bar{F}_k^{(1,2)}$ are bin-wise averages. The resulting estimated probability distributions p_i for each variable are normalized $\sum_{i=1}^Q p_i = 1$ with $0 \leq p_i \leq 1$. With this binned data, curves for the drift and diffusion coefficients can be directly plotted, see Refs. [5, 26]. However, the binning operation can lead to high relative errors in sparsely sampled regions and at the boundaries of the sampled phase space [26]. Therefore, we propose that the identification of SDEs can be improved by filtering out the binned data with high uncertainty. One way to implement such a filtering procedure is to simply fix a minimal probability threshold below which the data is removed.

In this work, we employ an entropy-based thresholding approach for automatic identification of the probability threshold [28]. The method is typically used for image processing, specifically for edge detection and image segmentation. It consists of two entropy-maximization steps for the Shannon- and Tsallis entropy, respectively. Maximization of the Shannon entropy produces thresholds that divide the data into “foreground” and “background”, corresponding to signal-dominated and noise-dominated phase-space regions, respectively. The threshold value is then improved in a second step by maximizing the Tsallis entropy of the “background”. Once the data is filtered, the equations for the KM coefficients, $D^{(1)}(x)$ and $D^{(2)}(x)$, are inferred by finding analytical expressions for $\bar{\mathbf{F}}^{(1,2)}$ as functions of $\bar{\mathbf{X}}$. For this purpose, a library $\Theta \in \mathbb{R}^{Q \times K}$ is constructed from the binned and filtered data, where Q is the number of bins and K is the number of terms in the library. For example, $\Theta = [\mathbf{1}, \bar{\mathbf{X}}, \bar{\mathbf{X}}^2, \dots, \sin(\bar{\mathbf{X}})]$. If the library contains all the function expressions necessary to describe the KM coefficients analytically, the governing equations can be written as

$$\bar{\mathbf{F}}^{(1)} = \Theta \mathbf{W}^{(1)}, \quad (14a)$$

$$\bar{\mathbf{F}}^{(2)} = \Theta \mathbf{W}^{(2)}, \quad (14b)$$

where $\mathbf{W}^{(1)}$ and $\mathbf{W}^{(2)}$ denote two sparse vectors whose non-zero entries correspond to the library terms to be included in the sought-for analytical expressions for the KM coefficients. Equation (14a) yields $D^{(1)}(x)$ and

Eq. (14b) yields $D^{(2)}(x)$. The inverse problems of finding optimal $\mathbf{W}^{(1,2)}$ in Eq. (14), have the same form as the problem in Eq. (2).

2. Estimation of KM coefficients without data binning

A more direct approach for estimating the KM coefficients is based on the use of the trajectories $\mathbf{F}_\ell^{(1)}$ and $\mathbf{F}_\ell^{(2)}$ without binning or filtering. For inference of the KM coefficients from space-time trajectories, we construct a library $\Theta \in \mathbb{R}^{N \times K}$, where N is the length of the trajectory and K is the number of terms in the library. For example, $\Theta = [\mathbf{1}, \mathbf{X}_1, \dots, \mathbf{X}_M, \mathbf{X}_1\mathbf{X}_2, \dots, \sin(\mathbf{X}_1), \dots]$. Under the assumption that the library contains all necessary terms describing the drift and diffusion coefficients, the coefficients for the ℓ -th component of the stochastic process can be inferred with

$$\mathbf{F}_\ell^{(1)} = \Theta \mathbf{W}_\ell^{(1)}, \quad (15a)$$

$$\mathbf{F}_\ell^{(2)} = \Theta \mathbf{W}_\ell^{(2)}, \quad (15b)$$

where $\ell \in \{1 \dots M\}$ and the vectors $\mathbf{W}_\ell^{(1,2)}$ are non-zero in those entries that correspond to the terms in the library that are required for the analytical description of the KM coefficient. The determination of the $\mathbf{W}_\ell^{(1,2)}$ is again an inverse optimization problem.

C. Automatic threshold sparse Bayesian learning

For identification of the relevant library terms as, e.g., for Eq. (15), we propose an algorithm that we call Automatic threshold sparse Bayesian learning (ATSBL). The method consists of two main steps. First, the inverse problem is solved with an efficient algorithm called Bayesian compressive sensing using Laplace priors (BCSL) [29]. Since the library is typically large, the solution vector generated by the BCSL algorithm typically still contains quite a few non-vanishing but small entries. Therefore, in a second step, the negligible contributions to the resulting governing equations are removed by an automatic thresholding procedure [3, 5, 7]. These two steps of the method are detailed below.

1. Bayesian compressive sensing using Laplace priors (BCSL)

We consider a generic linear equation system of the form

$$\mathbf{g} = \Phi \mathbf{w} + \mathbf{s}, \quad (16)$$

with a given vector \mathbf{g} and matrix Φ and an unknown, sparse vector \mathbf{w} . The vector \mathbf{s} represents noise or measurement errors. Various methods can be used to calculate sparse solution vectors \mathbf{w} from Eq. (16). In particular, research on compressive sensing, which deals

with the reconstruction of sparse signals from under-determined systems, has yielded powerful and efficient methods for finding sparse solution vectors \mathbf{w} . Among these are Bayesian methods based on the relevance vector machine (RVM) [30, 31]. Sparsely populated result vectors can be obtained by employing a Laplace distribution as prior probability distribution for \mathbf{w} . Here, we employ a method called Bayesian compressive sensing using Laplace priors (BCSL) [29]. Specifically, we employ a variant of BCSL that iteratively calculates approximate solutions [29], which is very computationally efficient and yields accurate results for our type of applications.

Briefly, the mathematical basis of BCSL is as follows. The method is based on a three-stage hierarchical model. It is assumed that the errors \mathbf{s} are drawn from a zero-mean Gaussian distribution with unknown variance $1/\beta$. Therefore, the likelihood function for finding a vector \mathbf{g} is given by

$$p(\mathbf{g}|\mathbf{w}, \beta) = \left(\frac{2\pi}{\beta}\right)^{-\frac{N}{2}} \exp\left\{-\frac{\beta}{2}\|\mathbf{g} - \Phi\mathbf{w}\|_2^2\right\}. \quad (17)$$

The unknown vector \mathbf{w} is assigned a prior distribution, which represents our knowledge on the nature of this quantity. To encode sparsity, one would like to employ a Laplace prior $p(\mathbf{w}|\lambda) = \lambda/2 \exp(-\lambda/2\|\mathbf{w}\|_1)$ with a hyperparameter λ . Evaluation of integrals using this choice of a Laplace prior is not readily accomplished, since the Laplace prior is not conjugate to the Gaussian likelihood, Eq. (17). Therefore, an auxiliary vector of hyperparameters γ with the same dimension as \mathbf{w} is employed to express the prior as the convolution of the two different distributions $p(\mathbf{w}|\gamma) = \prod_i \left[\exp(-w_i^2/(2\gamma_i^2))/(\sqrt{2\pi}\gamma_i)\right]$ and $p(\gamma|\lambda) = \prod_i [\lambda \exp(-\lambda\gamma_i/2)/2]$. These two distributions together result in a Laplace prior after marginalizing out γ as

$$p(\mathbf{w}|\lambda) = \int p(\mathbf{w}|\gamma)p(\gamma|\lambda)d\gamma = \frac{\lambda^{N/2}}{2^N} e^{-\sqrt{\lambda}\sum_i |w_i|}, \quad (18)$$

see Ref. [32]. Overall, the joint probability density results as

$$p(\mathbf{g}, \mathbf{w}, \gamma, \lambda, \beta) = p(\mathbf{g}|\mathbf{w}, \beta)p(\mathbf{w}|\gamma)p(\gamma|\lambda)p(\lambda)p(\beta). \quad (19)$$

To infer values for the most probable solution vector \mathbf{w} as well as the hyperparameters, an evidence procedure is employed wherein the posterior probability $p(\mathbf{w}, \gamma, \lambda, \beta|\mathbf{g})$ is maximized with respect to \mathbf{w} , γ , λ , and β , given the data. By making use of the expression

$$p(\mathbf{w}, \gamma, \lambda, \beta|\mathbf{g}) = p(\mathbf{w}|\mathbf{g}, \gamma, \lambda, \beta)p(\gamma, \lambda, \beta|\mathbf{g}) = \frac{p(\mathbf{g}, \mathbf{w}, \gamma, \lambda, \beta)}{p(\mathbf{g})} \quad (20)$$

together with Eq. (19), \mathbf{w} is determined by simply maximizing $p(\mathbf{g}|\mathbf{w}, \beta)p(\mathbf{w}|\gamma)$. This calculation yields for the result vector the expression $\mathbf{w}^* = \beta\Sigma\Phi^T\mathbf{g}$ with $\Sigma = (\beta\Phi^T\Phi + \Lambda)^{-1}$ with $\Lambda = \text{diag}(1/\gamma_i)$ [29]. This step corresponds to a Ridge regression that depends on the unknown values of γ , λ , and β . Determination of these

hyperparameters proceeds by maximizing

$$p(\gamma, \lambda, \beta | \mathbf{g}) = \frac{p(\gamma, \lambda, \beta, \mathbf{g})}{p(\mathbf{g})} \quad (21)$$

with respect to γ , λ , and β . Here, $p(\gamma, \lambda, \beta, \mathbf{g})$ is calculated from the right hand side of Eq. (19) by integrating out \mathbf{w} . With the fast, approximate version of BCSL, the equations determining the optimal values of the hyperparameters are solved iteratively, where only one entry of the vector γ is adjusted in every step.

2. Automatic thresholding

Solution of the inverse problem (16) with BCSL typically yields vectors \mathbf{w} that contain only a few large entries, but also a number of very small, non-zero entries. Removal of these negligible entries is desirable and we improve the solution sparsity with an iterative thresholding procedure [4]. The pseudocode 1 illustrates how the thresholding procedure proposed in in Ref. [4] is combined with BCSL proposed in Ref. [29]. Briefly, the thresholding algorithm works as follows. The input is given by \mathbf{g} , the library matrix Θ , an initial increment d_{tol} for the threshold tol , and the maximum number of iterations n_{iters} . The data \mathbf{g} and Θ is spilt into two parts for training and test, respectively. Usually, 80% of the data is used for training and 20% for testing. Thresholds are calculated iteratively from the training data and the validity of the thresholds is evaluated based on the error resulting from their application to the test data. The core part of the algorithm is a loop for iterative calculation of the sparse vector \mathbf{w} and the threshold tol . In each iteration step, the approximate, fast BCSL routine is first employed to obtain an estimate of \mathbf{w} from the training data. The quality of this solution estimate is evaluated by calculating the resulting error with the test data

$$e = \|\Theta^{\text{test}} \mathbf{w} - \mathbf{g}^{\text{test}}\|_2^2 + \eta \|\mathbf{w}\|_0, \quad (22)$$

where the penalty factor of the solution norm is chosen $\eta = 10^{-3} \kappa(\Theta)$ as suggested for the original algorithm [4]. If the error of the current solution is smaller than the error of previous iterations, the new solution is accepted and the threshold tol is increased. In the opposite case, the threshold is decreased and the increment d_{tol} is refined. The final solution \mathbf{w}_{best} is the sparse vector that determines the terms in the governing differential equations, SDEs, ODEs, and PDEs.

D. Quality score for identified governing equations

The error of the inference procedure can be directly quantified by comparison of the results with a known set of original differential equations in test cases. For this purpose, we define the deviation of identified coefficient

Function: ATSB $L(\Theta, \mathbf{g}, d_{\text{tol}}, n_{\text{iters}})$

%% Split data into parts for training and test
 $\Theta \mapsto [\Theta^{\text{train}}, \Theta^{\text{test}}]$ % ca. 80% training, 20% test
 $\mathbf{g} \mapsto [\mathbf{g}^{\text{train}}, \mathbf{g}^{\text{test}}]$

%% Initialization

$\sigma^2 = \text{var}(\mathbf{g}^{\text{train}})$ % Variance of data.

$\eta = 10^{-3} \kappa(\Theta)$ % $\kappa(\Theta)$ is condition number

$tol = d_{\text{tol}}$ % Initial threshold

$Q = \text{size}(\Theta, 2)$ % Number of library terms

$\mathbf{w}_{\text{best}} = (\Theta^{\text{train}})^{-1} \mathbf{g}^{\text{train}}$ % Initial solution guess

$e_{\text{best}} = \|\Theta^{\text{test}} \mathbf{w}_{\text{best}} - \mathbf{g}^{\text{test}}\|_2^2 + \eta \|\mathbf{w}_{\text{best}}\|_0$ % Initial error

%% Solution with iterative threshold adaptation

for ($i = 1; i < n_{\text{iters}}; i = i + 1$) {

$\hat{\mathbf{w}} = \text{FastBCSL}(\Theta^{\text{train}}, \mathbf{g}^{\text{train}}, \sigma^2)$

$\text{bigcoeffs} = \{m : |\hat{w}_m| \geq tol\}$

$\Theta^{\text{train}} = \Theta^{\text{train}}_{\text{old}}$;

$\Theta^{\text{train}} = \Theta^{\text{train}}(:, \text{bigcoeffs})$

if $i == 1$ **then**

$final_p = \text{bigcoeffs}$;

$\mathbf{w} = \hat{\mathbf{w}}$

else

$final_p = final_p(\text{bigcoeffs})$

$\mathbf{w} = \text{zeros}(Q, 1)$

$\mathbf{w}(final_p) = \hat{\mathbf{w}}(\text{bigcoeffs})$

end

% Calculate error and threshold

$e = \|\Theta^{\text{test}} \mathbf{w} - \mathbf{g}^{\text{test}}\|_2^2 + \eta \|\mathbf{w}\|_0$

% Adapt threshold

if $e \leq e_{\text{best}}$ **then**

% Error is decreasing. Increase threshold

$e_{\text{best}} = e$

$\mathbf{w}_{\text{best}} = \mathbf{w}$

$tol = tol + d_{\text{tol}}$

else

% Tolerance too high

$\Theta^{\text{train}} = \Theta^{\text{train}}_{\text{old}}$

$tol = \max([0, tol - 2d_{\text{tol}}])$

% Change threshold stepping

$d_{\text{tol}} = \frac{2d_{\text{tol}}}{n_{\text{iters}} - i}$

$tol = tol + d_{\text{tol}}$

end

}

return \mathbf{w}_{best}

Algorithm 1: Pseudocode for automatic threshold sparse Bayesian learning (ATSB L), which combines BCSL [29] and TrainSTRidge [4] to achieve parameter-free inference of highly sparse solutions to inverse problems.

(DIC) as

$$\text{DIC} = \frac{1}{K} \sum_i \frac{\|c_i - c'_i\|_2}{\max(\|c_i\|_2, \|c'_i\|_2)}, \quad (23)$$

where every c_i is a coefficient of one term in the identified equation and c'_i is the related coefficient in the original equation that was used to generate the test data. K represents the number of coefficients. Here, at least one of

the coefficients in each pair $\{c_i, c'_i\}$ is required to be non-zero and the sum only runs over these coefficients. The DIC lies in the range $[0, \infty]$ where 0 indicates a perfectly identified equation.

III. RESULTS

A. Inference of SDEs from noisy trajectories

We now illustrate the data-driven identification of SDEs by the example of overdamped Brownian motion of a particle inside a one-dimensional double-well potential with coordinate x . The drift and diffusion coefficients of this system are given by

$$D^{(1)}(x) = -2x^3 + 12x^2 - 18x + 3, \quad (24a)$$

$$D^{(2)}(x) = 0.8. \quad (24b)$$

The trajectory data that is to be used for inferring the governing equation is generated by integrating the Langevin equation with the Euler-Maruyama method. A trajectory \mathbf{X} is shown in Fig. (1-a-i) (10^6 time steps). The trajectories $\mathbf{F}^{(1)}$ and $\mathbf{F}^{(2)}$ are shown in Fig. (1-a-ii, iii). To visualize the x -dependence of the estimator for the drift coefficient, we plot $\mathbf{F}^{(1)}$ against \mathbf{X} , see Fig. (1-c-i). Similarly, $\mathbf{F}^{(2)}$ is plotted against \mathbf{X} as estimator of the diffusion coefficient $D^{(2)}(x)$ in Fig. (1-c-ii). Both plots exhibit large fluctuations around the true drift and diffusion coefficients and the resulting averages are clearly prone to errors, particularly at the boundaries of the sampled domain.

Using the trajectory data, we next construct a library consisting of 11 terms for the drift coefficient and 6 terms for the diffusion coefficient as illustrated in Fig. (1-b-i, ii). Then, we employ ATSBL to identify $\mathbf{W}^{(1)}$ and $\mathbf{W}^{(2)}$ directly from the trajectory without binning. The identified x -dependent functions for the drift and diffusion coefficients are plotted in Fig. (1-c-i, ii). They agree well with the original functions used for creating the data. The identified equations with estimated uncertainties are shown in Fig. (1-c).

The main distinction of ATSBL as compared to established inference techniques is the assumption of a Laplacian distribution for the prior of the library coefficients. The more direct, albeit theoretically less sparsity-promoting procedure is to employ a Gaussian prior, corresponding to a Ridge regression with fixed regularization parameter, for inference of the solution vector \mathbf{w} prior to thresholding, as done, e.g., in Ref. [4]. To compare the performance of these two approaches for inference of SDEs, we evaluate the deviation of the identified coefficients, DIC, as a function of the number of data points used for inference. The result that is shown in Fig. (1-d) indicates that the Laplacian prior leads to a faster convergence than the Gaussian prior. To further establish the robustness of ATSBL, we compare the convergence of the iterative thresholding procedure for each of the two

prior distributions. The result shown in Fig. (1-e-i, ii) demonstrate a better convergence achieved in the case of the Laplacian prior. For both, Gaussian and Laplacian prior distributions, the threshold and the error oscillate during the iteration process, which is due to the adaptive step size during the thresholding.

B. Inference of SDEs with time-dependent drift coefficient

In Sec. III A, an example is provided for how the KM coefficients can be obtained by performing a regression directly with data for a stochastic trajectory. The direct use of the trajectory data becomes particularly important for the treatment of the more complex situation of a time-varying force. In such a situation, the probability distribution in phase space changes over time, and it is not obvious how the dynamic distribution should be estimated from a single trajectory. Data binning is of no use in the case of time-dependent forces without the availability of ensembles of many trajectories for the same conditions. In order to explore the validity of our approach in this situation, we consider the example of a particle diffusing within a time-dependent one-dimensional potential. The drift and diffusion coefficients of this system are given by

$$D^{(1)}(x) = [a_0 + 1 - \cos(\omega t)]x - x^3, \quad (25a)$$

$$D^{(2)}(x) = 0.8. \quad (25b)$$

with $a_0 = 5 \times 10^{-3}$. The potential has a double-well shape, where the positions of the two minima vary periodically in time. The two minima start at separate positions and merge periodically into one minimum before separating again to reach the initial positions. Each time the potential wells come close to each other, the transition probability becomes large and the particle is likely to change from one well to another. This gives rise to stochastic oscillations between the two potential wells. To test whether the underlying equations can be inferred with a library constructed from a single trajectory, we assume that the frequency ω at which the potential changes is known. Inference of this frequency from the data is in principle also possible, but requires excessive computational power since high-order terms with explicit time-dependence must be accounted for in the library. We construct a library consisting of a time-dependent and a time-independent part. The first half of the library is simply a polynomial basis, the second half corresponds to the polynomial basis multiplied with a $\cos(\omega t)$ factor. The results of the inference procedure are shown in Fig. (2-a). The inferred equation is in agreement with the correct equation. For illustration, we plot snapshots of the force field for fixed time for the original equations and the inferred equations.

The fact that the inference procedure shows a remarkable performance even though the derivatives have been

calculated from noisy trajectories may at first sight seem counter-intuitive. We remark that this result is to be attributed to the Gaussian nature of the noise, because in the present case the non-linearities of the library functions are exact and there is no non-linear amplification of noise. Thus, as long as the trajectory is long enough to allow for an efficient sampling of phase space, the derivatives can be calculated from noisy trajectories and the inference procedure is expected to be reliable.

C. Data binning for inference of SDEs from short trajectories

The method of inferring of SDEs with the help of libraries that are directly constructed from trajectory data can become unreliable when confronted with short trajectories in an inhomogeneous force field. In such a situation, we find that it is more appropriate to apply a filtering procedure to the data. We illustrate this procedure with the case of overdamped Brownian diffusion with space-dependent diffusion coefficient in a one-dimensional double-well potential. The drift and diffusion coefficients of the model are given by

$$D^{(1)}(x) = -2x^3 + 12x^2 - 18x + 3, \quad (26a)$$

$$D^{(2)}(x) = x^2 - 2x + 2. \quad (26b)$$

We first consider short trajectories that have $2 \cdot 10^5$ time steps, illustrated exemplarily in Fig. (2-b-i). The raw data and binned data are, respectively, plotted in Fig. (2b-ii, iii) and Fig. (2b-v, vi). The distribution of the binned data (bins = 200) clearly deviates from the known functions of $D^{(1,2)}(x)$ in undersampled regions. Therefore, the binned data is filtered to remove data points with high uncertainty. This filtering is done as described in Sec. IIB 1 by removing the bins below a probability threshold \hat{p}^T determined by entropy maximization [28], see Fig. (2-b-v, vi). To assess if binning and filtering is also beneficial for long trajectories, we also use data from trajectories with $2 \cdot 10^7$ time steps. Figure (2-b-vii) shows the errors of the identified coefficients.

For short trajectories, binning is advantageous in combination with a filtering procedure to suppress data with high uncertainty. In this case, we find that the identified equations have the correct terms as compared to original equations. This procedure yields better results than the direct use of the trajectory data in the case of short trajectories. The reason for this finding can be understood from Fig. (2b-v, vi), where the inferred functions match to the correct functions only in the most populated regions of phase space. Thus, the exclusion of data points with high uncertainty can drastically improve the inference of underlying dynamical equations if the trajectory is not long enough to allow sufficient sampling of the phase space. Conversely, for the long trajectory we find that both procedures yield governing equations containing the correct terms.

D. Active sampling with feed-back perturbation improves identification of SDEs

We have so far restricted our attention to the extraction of estimates from a given set of experimental data. Thereby, we have assumed that the size of the data set is large enough to allow some form of inference of the governing equations. In a different scenario one might have the ability to perturb the studied system, either in a computer simulation or in an experimental setup, while simultaneously recording the data. In such a scenario, one may enhance the sampling efficiency by means of an appropriately designed perturbation that is applied to the system. This kind of methodology has proved useful for example in the context of computational studies of nucleation [33] and growth [34] processes. Generally, this methodology is expected to be useful whenever the systems dynamics is governed by an energy landscape with multiple local minima and when the trajectory is trapped at one particular local minimum of the energy landscape. We describe an adaptive control method, where the simultaneous inference of the dynamical equations together with a perturbation of the system recursively result in an exploration of the global structure of phase space to provide sufficient sampling everywhere.

Since the phase space probability distribution generally tends to be peaked around local minima of the potential, the dynamical equations can be estimated locally near these minima. To take advantage of this local estimation and iteratively extend the sampled phase space region, we re-sample the trajectory repeatedly while applying a control force that is opposite to the locally estimated force. The difficulty with a straight-forward application of this method is that the control force can admit large deviations away from the initial estimation region. This effect produces large errors, slows down convergence, and may even lead to divergence problems. We overcome this problem by weighting the control force with a Gaussian distribution such that the control force vanishes away from the current estimation region, while it is directly opposite to the estimated force at estimation regions. Thus, the control force will effectively expel the trajectory from the local minimum where the estimation has been performed and the trajectory will eventually reach another local minimum.

The method, which we call automatic iterative sampling optimization (AISO), is illustrated in Fig. (3-a-i-iv) and the pseudocode is provided in Algorithm 2. At each iteration, the underlying dynamical equations are estimated from the data accumulated during all previous iterations. The negative of the inferred drift term is employed locally as control force. The center and width of the Gaussian weight of the control force is calculated only from the mean and standard deviation of the trajectory of the previous step. Thus, we formally define our

control force acting on the component ℓ as

$$c_\ell^i(\{X_{\ell'}(t)\}) = -\Theta_\ell(\{X_{\ell'}(t)\}) \cdot \mathbf{w}^i \exp\left[-\frac{\|X_\ell(t) - \mu_\ell^i\|^2}{\zeta_\ell^i}\right] \quad (27)$$

where the index i indicates that values are to be taken at the iteration number i ; μ_ℓ^i and ζ_ℓ^i stand for the mean and variance of the trajectory extracted from the step i in each iteration. After a sufficient number of iterations, the data points accumulated from all iterations are combined and the equation of motion is extracted from the accumulated data. This procedure is repeated for a predefined number of iteration steps. For the examples presented in the following, the iteration step number has been fixed to $N = 10$, since convergence has been achieved within less than 10 steps in these cases.

For a first demonstration of our method, we employ a three-well potential $U(x) = x^6 - 6x^4 + 0.5x^3 + 8x^2$ with a constant diffusion coefficient for simulating the trajectory of a particle in one dimension. The drift and diffusion coefficients are

$$D^{(1)}(x) = -\frac{dU}{dx} = -6x^5 + 24x^3 - 1.5x^2 - 16x, \quad (28a)$$

$$D^{(2)}(x) = 1. \quad (28b)$$

Next, we also consider a two-dimensional drift field, consisting of a radially symmetric component and a shear component in the x, y -plane. The drift and diffusion coefficients are given by

$$D_x^{(1)}(x, y) = x(1 - x^2 - y^2) + y(x^2 - y^2 - b) \quad (29a)$$

$$D_y^{(1)}(x, y) = y(1 - x^2 - y^2) + x(x^2 - y^2 - b), \quad (29b)$$

$$D_x^{(2)}(x, y) = D_y^{(2)}(x, y) = 1. \quad (29c)$$

Using these driving forces, we simulate trajectories with 10^5 time steps with one time step being $\Delta t = 5 \cdot 10^{-3}$. A part of the trajectory on the potential map is illustrated Fig. (3-b-i, vi). Results for the intermediate iteration steps are shown together with the drift field in Fig. (3-b-iii, vi). As iterations of the algorithm proceed, the coefficients of the control potential are approaching the coefficients of the correct drift field, and the expulsion from each local minimum becomes more efficient. This results in an enhancement of rare events where the particle crosses the saddle points, as illustrated in Fig. (3-b-i, vi) by the controlled and uncontrolled trajectories. Using ATSBLL, we identify $\tilde{D}^{(1)}(x)$ and $\tilde{D}^{(2)}(x)$ in each iteration. The DIC reduces from 1 to nearly 0.01 during the iterations, as illustrated in Fig. (3-b-ii, v). Thus, the terms of the identified equations approach those given in the original equations.

E. Identification of ordinary and partial differential equations

Next, it is shown that the sparse inference scheme based on Laplace priors implemented in ATSBLL can also

Function: AISO()

```

 $\mathbf{c}^0 = \mathbf{0}$ ; %Initialize control force to zero
N = 10; %Fix number of iteration steps
i = 0; %Initialize iterator to zero
while i < N do
    i = i + 1;
    %For all degrees of freedom  $\ell, \ell' \in \{1 \dots M\}$ 
    %Add control force and generate data
     $\frac{dX_\ell(t)}{dt} = g_\ell(\mathbf{X}(t), t) + c_\ell^{i-1} + \sum_{\ell'} h_{\ell, \ell'}(\mathbf{X}(t), t) dW_{\ell'}(t)$ 
    %Subtract control force and collect data
     $\frac{dX_\ell(t)}{dt} \leftarrow \frac{dX_\ell(t)}{dt} - c_\ell^{i-1}$ 
    %Concatenate data
     $\Theta \leftarrow (\Theta, \Theta(X_\ell(t)))$ 
     $\mathbf{g} \leftarrow (\mathbf{g}, \frac{dX_\ell(t)}{dt})$ 
    %Estimate library coefficients with ATSBLL
     $\mathbf{w} = \text{ATSBLL}(\Theta, \mathbf{g}, d_{\text{tol}}, n_{\text{iters}})$ 
end
return  $\mathbf{w}$ 

```

Algorithm 2: Pseudocode for identification of SDEs with automatic iterative sampling optimization (AISO)

be used for data-driven discovery of ordinary and partial differential equations. The identification of ODEs from trajectory data is demonstrated with a Lorenz system, which is a paradigm for chaotic behaviour [35]. The Lorenz equations are given by

$$\dot{x} = a(y - x), \quad (30a)$$

$$\dot{y} = x(b - z) - y, \quad (30b)$$

$$\dot{z} = xy - cz, \quad (30c)$$

where the parameters are fixed as $a = 10$, $b = 28$, and $c = 3/8$. We numerically integrate these equations to obtain a trajectory as shown in Fig. (4-a). The chaotic system involves two attractors. For data-driven system identification, we utilize three identical libraries Θ for each of the variables, x , y and z . Θ is constructed from the simulated trajectory and includes 56 terms containing up to fourth powers of all variables. Time-derivatives are calculated using the finite-difference approximation. The general ODEs constructed from the library are represented by three linear equations, as in Eq. (4). For the noise-free data, the equations that are inferred from the data with ATSBLL are within a relative error of order of 10^{-4} , as shown in Fig. (4-b). The same inference procedure is then repeated for a trajectory with additional Gaussian noise. The standard deviation of the noise in each coordinate is chosen to be 2 % of the standard deviation of the data range in that coordinate. For this case, the ODEs identified with ATSBLL still contain all the correct terms and errors in the inferred system parameters are in the percent range, see Fig. (4-b).

Finally, we demonstrate data-driven discovery of PDEs with ATSBLL. Reaction-diffusion equations have attracted interest as prototypic models for pattern formation in biochemical systems, where constituents are locally transformed into each other through chemical re-

actions and transported in space by diffusion. Here, we consider the popular $\lambda - \omega$ system, given by

$$\begin{aligned} u_t &= D_u \nabla^2 u + \lambda(A)u - \omega(A)v, \\ v_t &= D_v \nabla^2 v + \omega(A)u + \lambda(A)v, \\ A &= u^2 + v^2, \quad \omega = -\beta A^2, \quad \lambda = 1 - A^2, \end{aligned}$$

where β is equal to 2. A two-dimensional, planar, rectangular area with periodic boundary conditions is considered. The initial values of u and v are shown in Figs. (5-a-i, ii). The reaction-diffusion equations are solved numerically by using a spectral method. Snapshots of u and v are shown in Figs. (5-a-iii, iv). For inference of the governing PDEs, a library matrix Θ is constructed containing 35 terms each for u_t and v_t . Then, using ATSBL, the reaction-diffusion equations are inferred from the simulated data, as illustrated in Fig. 5(b). For noise-free data, the identified equations deviate from the original equations only at the fourth decimal place and this error is due to discretization. However, if u and v are corrupted with additive noise, identification of the correct PDEs becomes challenging [4]. In Ref. [4], it has therefore been suggested to include a denoising step prior to the inference step. Accordingly, we employ a curvelet denoising method [36], which permits reconstruction of the reaction-diffusion equations from data with 2% noise with ATSBL, as illustrated in Fig. 5(b).

IV. SUMMARY AND OUTLOOK

Data-driven, automatic discovery of governing equations has become a viable tool for studying complex systems if first-principle derivations are intractable, e.g., for biological systems or epidemiological data. The aim is here generally to construct an analytical model that characterizes the observed dynamics and extends to parameter- and phase space regions that are hard to access experimentally.

Our main contribution is a inference method that makes use of Laplacian prior distributions in a Bayesian framework to find a minimal set of governing equations without the need for user input. We establish the validity of this approach and compare it to other methods. Regarding data-driven discovery of SDEs, we show that the binning of trajectory data is only advantageous for inference of drift and diffusion coefficients if the sampled trajectories are insufficient to cover the whole phase space. In that case, the precision of the inference procedure is subject to considerable variation with respect to different phase-space regions, due to the varying probability weight. Here, we note that a filtering procedure consisting of the exclusion of data with high uncertainty in conjunction with data binning leads to significantly improved inference accuracy.

Next, we investigate how active learning procedures can be useful in situations where inference of global governing equations becomes impossible due to the trap-

ping of the trajectory within local phase space regions. Well-established umbrella sampling consists of adding quadratic bias potentials to reduce the energetic barriers in the original potential landscape [17, 37]. Introduction of such bias potentials has the inconvenience that extra parameters are needed to define the bias potential. Moreover, if the bias potentials are employed to smoothen the potential landscape, their appropriate placement in phase space needs to be determined. Here, we employ data-driven identification of governing equations for calculating time-dependent external perturbations that force the trajectory to explore the full phase space. The main feature of our method is that the parameters defining the control force correspond to the parameters defining the potential surface to be estimated. This method of active learning results in significant improvements of the quality of the inferred governing equations. We expect that the concept of active learning proposed in this work will extend the applicability of data-driven equation-discovery methods, in particular in the context of computer simulations.

An important future challenge for improving the library-based methodology for data-driven identification of analytical models is to find automated approaches for tailoring the employed function space to the problem at hand. Recent advances in the development of data-driven methods [38] suggest that a possible solution to the problem related to library construction is to integrate physical constraints, such as symmetries, conservation laws, or even thermodynamics in a generic framework for statistical learning. Data-driven identification of analytical models thus has the potential to become a popular tool for closing the gap between non-parametric, empirical modeling and first-principles-based modeling in the coming years.

ACKNOWLEDGMENTS

Funding by the European Research Council through a starting grant for BS is acknowledged (BacForce, g.a.No. 852585).

AUTHOR CONTRIBUTIONS

All authors designed the study, performed the research and wrote the manuscript together.

COMPETING INTERESTS

The authors declare no competing interests.

DATA AVAILABILITY

Source code and data can be obtained from the corresponding author upon request.

-
- [1] M. Schmidt and H. Lipson, Distilling free-form natural laws from experimental data, *Science* **324**, 81 (2009).
- [2] J. Bongard and H. Lipson, Automated reverse engineering of nonlinear dynamical systems, *Proc. Natl. Acad. Sci. U.S.A.* **104**, 9943 (2007).
- [3] S. L. Brunton, J. L. Proctor, and J. N. Kutz, Discovering governing equations from data by sparse identification of nonlinear dynamical systems, *Proc. Natl. Acad. Sci. U.S.A.* **113**, 3932 (2016).
- [4] S. H. Rudy, S. L. Brunton, J. L. Proctor, and J. N. Kutz, Data-driven discovery of partial differential equations, *Sci. Adv.* **3**, e1602614 (2017).
- [5] L. Boninsegna, F. Nüske, and C. Clementi, Sparse learning of stochastic dynamical equations, *J. Chem. Phys.* **148**, 241723 (2018).
- [6] M. Raissi, A. Yazdani, and G. E. Karniadakis, Hidden fluid mechanics: Learning velocity and pressure fields from flow visualizations, *Science* **367**, 1026 (2020).
- [7] S. Zhang and G. Lin, Robust data-driven discovery of governing physical laws with error bars, *Proc. Math. Phys. Eng.* **474**, 20180305 (2018).
- [8] R. Friedrich, J. Peinke, M. Sahimi, and M. R. R. Tabar, Approaching complexity by stochastic methods: From biological systems to turbulence, *Phys. Rept.* **506**, 87 (2011).
- [9] G. J. Stephens, M. B. De Mesquita, W. S. Ryu, and W. Bialek, Emergence of long timescales and stereotyped behaviors in *Caenorhabditis elegans*, *Proc. Nat. Acad. Sci. USA* **108**, 7286 (2011).
- [10] R. Sarfati, J. Bławdziewicz, and E. R. Dufresne, Maximum likelihood estimations of force and mobility from single short brownian trajectories, *Soft Matter* **13**, 2174 (2017).
- [11] L. Pérez García, J. Donlucas Pérez, G. Volpe, A. V Arzola, and G. Volpe, High-performance reconstruction of microscopic force fields from brownian trajectories, *Nat. Commun.* **9**, 1 (2018).
- [12] M. Baldovin, A. Puglisi, and A. Vulpiani, Langevin equations from experimental data: The case of rotational diffusion in granular media, *PloS one* **14**, e0212135 (2019).
- [13] A. Frishman and P. Ronceray, Learning force fields from stochastic trajectories, *Phys. Rev. X* **10**, 021009 (2020).
- [14] F. Ferretti, V. Chardès, T. Mora, A. M. Walczak, and I. Giardina, Building general langevin models from discrete datasets, *Phys. Rev. X* **10**, 031018 (2020).
- [15] D. B. Brückner, P. Ronceray, and C. P. Broedersz, Inferring the dynamics of underdamped stochastic systems, *Phys. Rev. Lett.* **125**, 058103 (2020).
- [16] D. B. Brückner, N. Arlt, A. Fink, P. Ronceray, J. O. Rädler, and C. P. Broedersz, Learning the dynamics of cell-cell interactions in confined cell migration, *Proc. Nat. Acad. Sci. USA* **118** (2021).
- [17] G. M. Torrie and J. P. Valleau, Nonphysical sampling distributions in monte carlo free-energy estimation: Umbrella sampling, *J. Comput. Phys.* **23**, 187 (1977).
- [18] O. Valsson and M. Parrinello, Variational approach to enhanced sampling and free energy calculations, *Phys. Rev. Lett.* **113**, 090601 (2014).
- [19] J. F. Dama, M. Parrinello, and G. A. Voth, Well-tempered metadynamics converges asymptotically, *Phys. Rev. Lett.* **112**, 240602 (2014).
- [20] M. Invernizzi, P. M. Piaggi, and M. Parrinello, Unified approach to enhanced sampling, *Phys. Rev. X* **10**, 041034 (2020).
- [21] G. Besold, J. Risbo, and O. G. Mouritsen, Efficient monte carlo sampling by direct flattening of free energy barriers, *Comput. Mat. Sci.* **15**, 311 (1999).
- [22] S. Goedecker, Minima hopping: An efficient search method for the global minimum of the potential energy surface of complex molecular systems, *J. Chem. Phys.* **120**, 9911 (2004).
- [23] H. Risken, Fokker-planck equation, in *The Fokker-Planck Equation* (Springer, 1996) pp. 63–95.
- [24] J. Náprstek and R. Král, Multi-dimensional fokker-planck equation analysis using the modified finite element method, in *J. Phys. Conf. Ser.*, Vol. 744 (2016) p. 012177.
- [25] C. Honisch and R. Friedrich, Estimation of kramers-moyal coefficients at low sampling rates, *Phys. Rev. E* **83**, 066701 (2011).
- [26] P. Rinn, P. Lind, M. Wächter, and J. Peinke, The langevin approach: An r package for modeling markov processes, *J. Open Res. Software* **4** (2016).
- [27] J. Gradišek, S. Siegert, R. Friedrich, and I. Grabec, Analysis of time series from stochastic processes, *Phys. Rev. E* **62**, 3146 (2000).
- [28] M. A. El-Sayed, A new algorithm based entropic threshold for edge detection in images, *International Journal of Computer Science Issues (IJCSI)* **8**, 71 (2011).
- [29] S. D. Babacan, R. Molina, and A. K. Katsaggelos, Bayesian compressive sensing using laplace priors, *IEEE Trans. Image Process.* **19**, 53 (2009).
- [30] M. E. Tipping, Sparse bayesian learning and the relevance vector machine, *J. Mach. Learn. Res.* **1**, 211 (2001).
- [31] S. Ji, Y. Xue, and L. Carin, Bayesian compressive sensing, *IEEE Trans. Signal* **56**, 2346 (2008).
- [32] M. A. Figueiredo, Adaptive sparseness for supervised learning, *IEEE Trans. Pattern Anal. Mach. Intell.* **25**, 1150 (2003).
- [33] R. Blaak, S. Auer, D. Frenkel, and H. Löwen, Crystal nucleation of colloidal suspensions under shear, *Phys. Rev. Lett.* **93**, 068303 (2004).
- [34] K. Klymko, P. L. Geissler, J. P. Garrahan, and S. Whitley, Rare behavior of growth processes via umbrella sampling of trajectories, *Phys. Rev. E* **97**, 032123 (2018).
- [35] E. N. Lorenz, Deterministic nonperiodic flow, *J. Atmos. Sci.* **20**, 130 (1963).
- [36] G. Peyré, The numerical tours of signal processing-advanced computational signal and image processing, *IEEE Comput. Sci. Eng.* **13**, 94 (2011).

- [37] G. Bussi and A. Laio, Using metadynamics to explore complex free-energy landscapes, *Nat. Rev. Phys.* , 1 (2020).
- [38] G. E. Karniadakis, I. G. Kevrekidis, L. Lu, P. Perdikaris, S. Wang, and L. Yang, Physics-informed machine learning, *Nat. Rev. Phys.* **3**, 422 (2021).

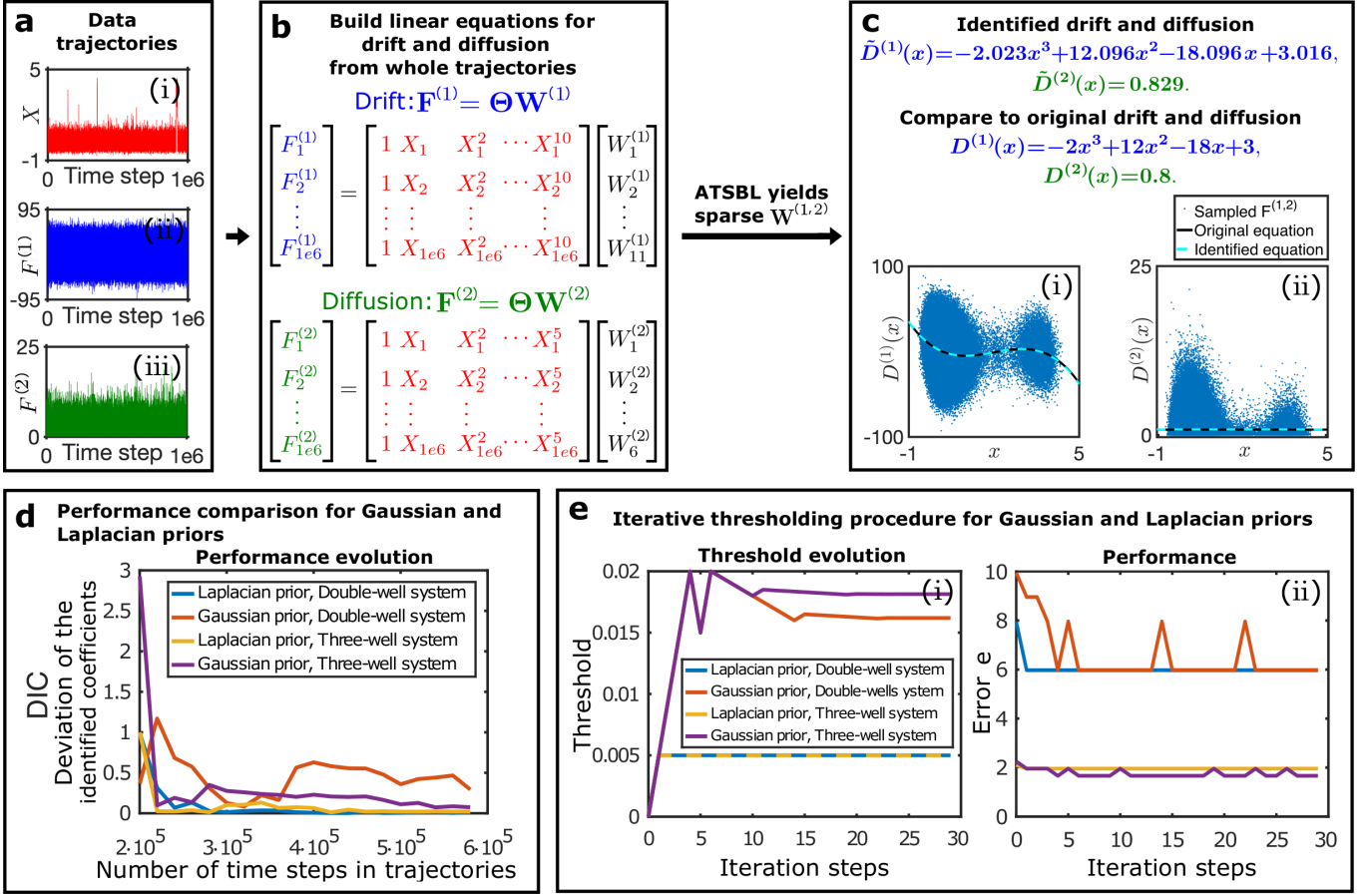


FIG. 1. Data-driven discovery of a one-dimensional SDE with automatic threshold sparse Bayesian learning (ATSBL). (a-i) Trajectory of a particle undergoing overdamped diffusive motion in a double-well potential (10^6 time steps). (a-ii, a-III) Time-series of the discrete differences and squared discrete differences for the same trajectory. (b) By evaluating function libraries by using the trajectory data, linear equations are constructed that relate known sequences of $\mathbf{F}^{(1,2)}$ to unknown, sparse set of coefficients $\mathbf{W}^{(1,2)}$ that determine the library terms (functions) that are required to describe $D^{(1,2)}$. (c) Exemplary results of the inference procedure. Despite the high noise amplitude, accurate predictions can be made directly from the trajectory data. (d) Comparison of the use of a Laplacian and Gaussian prior distribution in the inference procedure. The deviation of the identified coefficient (DIC) for the drift coefficient is plotted against the number of data points used for training. The Laplace prior in ATSBL decreases the error and reduces the required sample size. (e) Convergence rate of the thresholding procedure for Laplacian and Gaussian prior distributions. (e-i) Laplace priors result in fast threshold convergence. (e-ii) The error e defined in Eq. (22) decreases during the iterations. Errors achieved with Gaussian- and Laplacian priors are comparable.

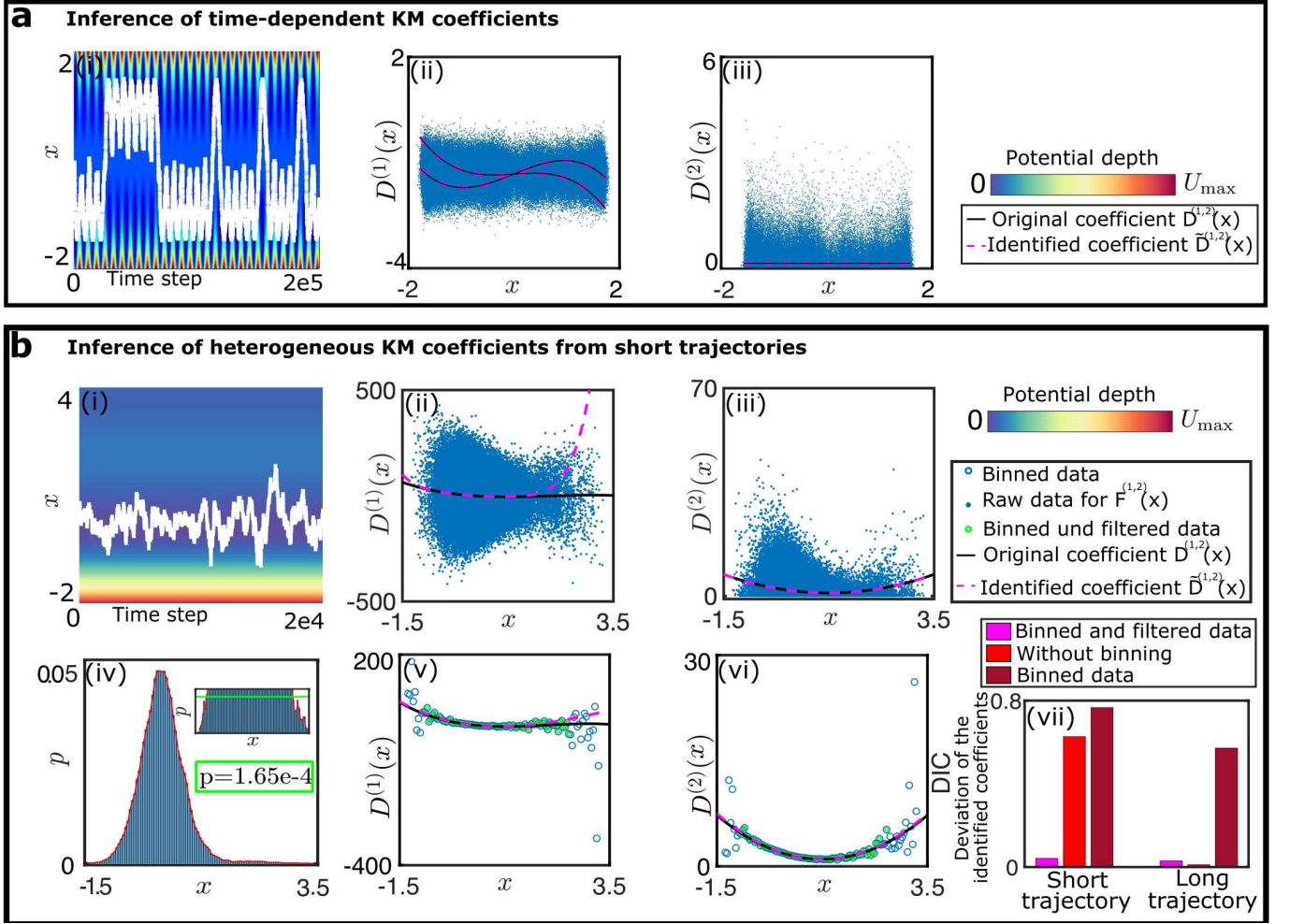


FIG. 2. Inference of KM coefficients for complex one-dimensional SDEs. (a) Time-dependent force field. (a-i) Trajectory of an overdamped motion in a time-varying double-well potential. (a-ii, iii) Using an appropriate function library, the functional forms of the KM coefficients can be faithfully reconstructed. (b) Inference KM coefficients from short trajectories. (b-i) Trajectory resulting from overdamped motion in a double-well potential with space-dependent diffusion coefficient. (b-ii, iii) Inferred x -dependence of coefficients with raw data for $F^{(1,2)}$ for short trajectories (2×10^5 time steps). The unpopulated regions in phase space are characterized by a high uncertainty of inference and therefore lead to large deviations in the coefficients. (b-iv) Histogram of particle positions for the trajectory shown in (i). (b-iv, v, vi) Binned distributions can be used to infer the KM coefficients, but large errors occur in regions that are not well-sampled. Inference errors due to incomplete phase-space sampling for short trajectories can be accounted for by excluding the data below a probability threshold, corresponding to large uncertainty. (b-vii) Performance of the inference with data binning and without data binning for short and long trajectories (2×10^5 and 2×10^7 time steps, respectively). The shown DIC is the average of the DICs for $D^{(1)}$ and $D^{(2)}$. For long trajectories, data binning does not reduce the error.

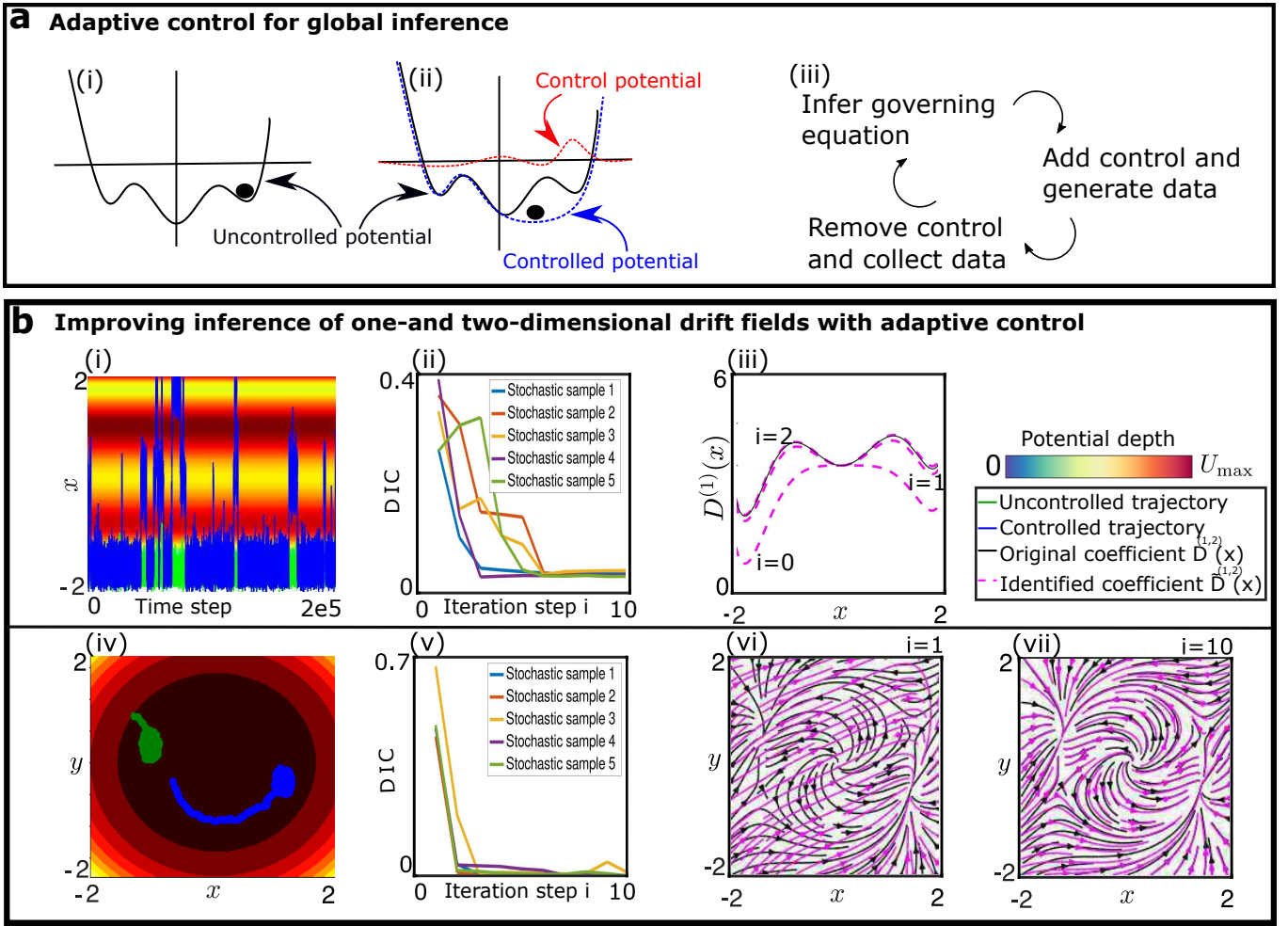


FIG. 3. Active learning with automatic iterative sampling optimization (AISO). (a) Schematic presentation of automatic iterative sampling optimization for the case of Brownian diffusion (a-i). Initially, the particle is trapped in one local minimum of the potential surface and the functional form of this potential can only be inferred locally. (a-ii) After the first iteration step, the potential surface near the estimated minimum is flattened and the particle is allowed to explore other regions in phase space. The same procedure is repeated iteratively and the control is always applied at the minimum estimated during the previous iteration. (a-iii) Schematic representation of the main feedback control loop. (b-i) Trajectory of a particle undergoing Brownian motion in a one-dimensional three-well potential. The black curve shows the uncontrolled trajectory, while the blue curve shows an example of a controlled trajectory. (b-ii) The deviation of the inferred coefficients (DIC) decreases during the iterations. (b-iii) The identified drift field converges to the original function during the iteration. (b-iv) Trajectory of a particle undergoing diffusion in a two-dimensional force field. The green curve exemplifies a trapped trajectory for plain sampling. The blue curve shows an example of a trajectory in the presence of control forces. Note that the colour of the background only indicates the potential $V(x, y) = -1/2(x^2 + y^2) + 1/4(x^2 + y^2)^2$, not the full force field. (b-v) Decrease of the DIC during the iteration. (b-vi) Streamlines of identified drift field (pink) and streamlines of the correct drift field (black) after the first iteration. (b-vii) Streamlines of identified drift field (pink) and streamlines of the correct drift field (black) after the tenth iteration. The identified force field now closely matches the original one.

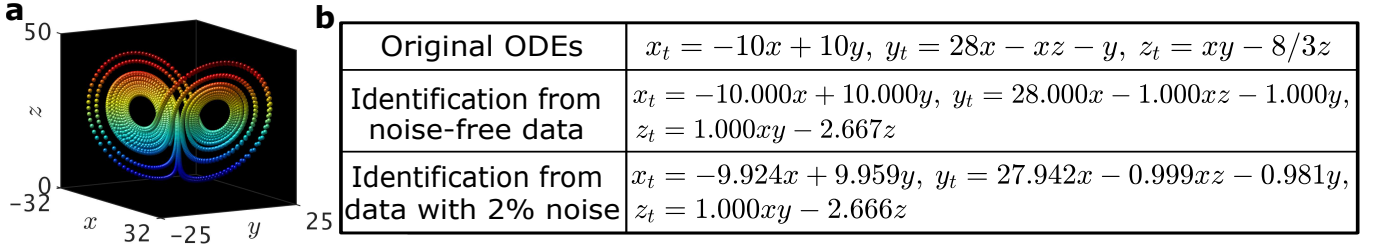


FIG. 4. Example for data-driven discovery of ODEs with ATSBL. (a) Plot of a numerically integrated trajectory for $t \in [0, 25]$ with a time step of $\Delta t = 2 \cdot 10^{-4}$ and an initial condition as $[x_0, y_0, z_0] = [-8, 8, 27]$. (b) The table shows the original ODEs, i.e., the Lorenz system, and the identified ODEs from noise-free-data and data with 2% Gaussian noise.

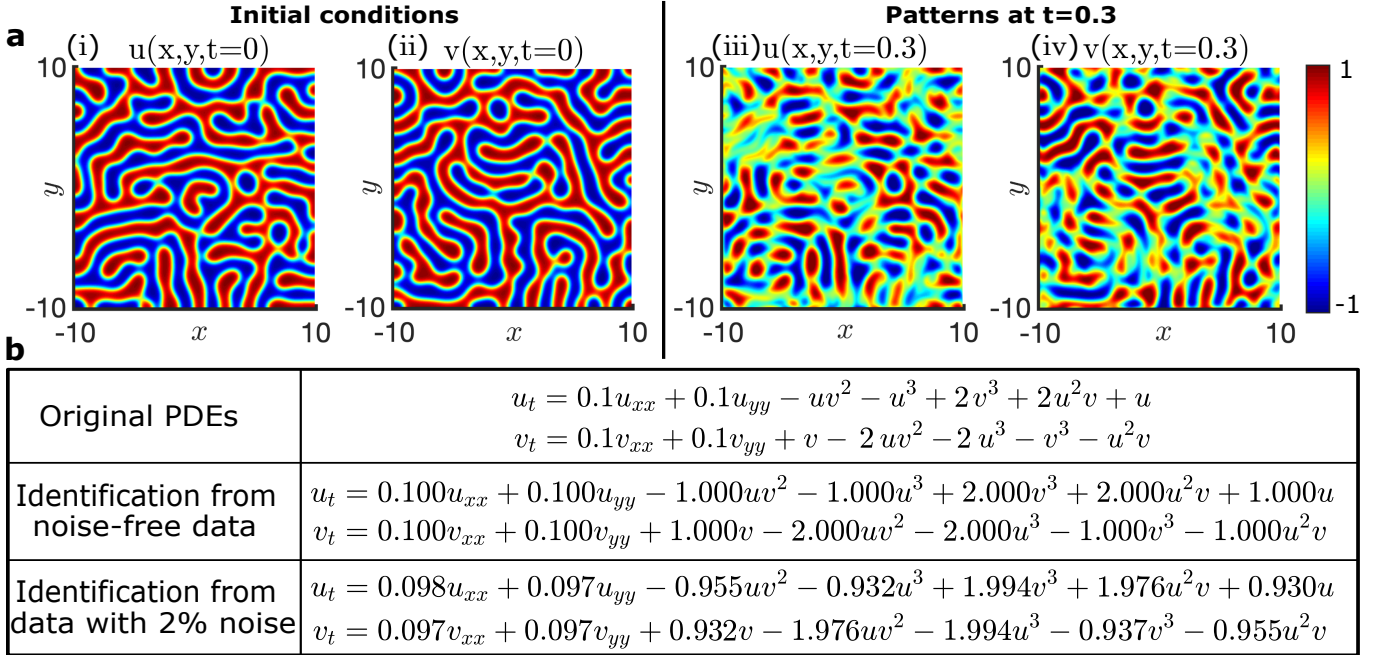


FIG. 5. Example for data-driven discovery of PDEs with ATSBL, using a reaction-diffusion system. (a-i, ii) Snapshots of the initial conditions for the variables u and v , respectively. (a-iii, iv) u and v at time $t = 0.3$. (b) The table shows the original PDEs for the reaction-diffusion system and the identified PDEs for noise-free data and data with 2% Gaussian noise. Inference is conducted with a library containing 35 terms. The numerical calculations are done with a time step $\Delta t = 0.0034$ in the time interval $t = [0, 0.6]$. The space domain has size 20×20 and is covered with a 256×256 grid with periodic boundary conditions.